SYSTEM CALIBRATION OF LAND-BAED MOBILE MAPPING SYSTEMS

By
Taher Hassan and Naser El-Sheimy
Mobile Multi-sensor Research Group
Department of Geomatics Engineering,
The University of Calgary
2500 University Dr. N.W. Calgary, Alberta, Canada T2N 1N4
Tel: (403) 220 7587, Fax: (403) 284 1980
E-mail: tfabbas@ucalgary.ca, naser@geomatics.ucalgary.ca

KEY WORDS: Mobile Mapping, Photogrammetry, Boresight Calibration, bundle Adjustment.

ABSTRACT:

The increasing demand for up-to-date 3-D geographic information systems (GIS) data for planning, transportation, and utility management applications poses significant challenges to the Geomatics community. Of all the challenges in acquiring, building, maintaining, and using GIS, none is more central than that of data acquisition. Obtaining the required spatial and attribute data by conventional methods such as aerial photogrammetry and terrestrial surveying is expensive and time consuming. These methods are, therefore, not well suited for rapid updating of GIS databases. Fortunately, the development of land-based mobile mapping systems (MMS) has opened a new avenue to meet these challenges. Land-based MMS are capable of providing fast, efficient, cost-effective and complete data acquisition systems. As such, they are an innovative technology for creating and updating 3-D GIS databases both quickly and inexpensively.

The delivered accuracy of MMS is a function of several parameters. This includes the accuracy of the navigation component which provides the absolute location and orientation of the system. Individual sensor calibration provides models for correcting their measurements systematic errors. Total system calibration is a key factor in MMS performance. In this step, the geometric relationship between the mapping sensor and the navigation sensor is estimated. This involves the determination of the camera perspective centre location with respect to the Inertial Navigation Systems (INS) triad centre which is typically part of the navigation component. Also, the rotation angles between the camera axes and the INS axes are estimated.

In this paper, we report our experience in calibrating the VISAT ^{TM} (**V**ideo-**I**nertia-**SAT**ellite) mobile mapping system which is developed by Absolute Mapping Solution Inc. The paper presents the different alternatives in boresight calibration. A project recently finished in Calgary, Canada, provided the opportunity to test the system under different field conditions. Results of these tests are reported in this paper with more emphasis on the impact of system calibration on the absolute and relative accuracy of the VISAT system.

1. INTRODUCTION

Mobile mapping systems (MMS) provide a complete mapping solution with data acquired from only one platform. The idea of mobile mapping has been around for at least as long as photogrammetry has been practiced. The early development of mobile mapping systems was, however restricted to applications that permitted the determination of the elements of exterior orientation from existing ground control. However, technological advancement in positioning/navigation and imaging sensors substantially refined the concept of airborne and land-based mapping. The advent of the first mobile mapping system in the early 1990s initiated the process of establishing modern, fully digital, virtually ground control-free photogrammetry and mapping, which considerably enhanced both the efficiency, the flexibility and the cost (after Schwarz and El-Sheimy, 2004).

The calibration of a MMS is an essential step prior to using the system in operational environment. It can be divided into two parts: calibration of each individual sensor and total system calibration (i.e. calibration of the spatial relation between different sensors). Camera calibration includes the estimation of the camera principle distance, the shift of the principle point, and the lens distortion parameters, which usually refereed to as internal orientation parameters. Inertial Navigation Systems (INS) are subjected to different calibration tests to estimate their sensors systematic errors (e.g. biases, temperature sensitivity, and scale factors).

VISAT was among the earliest MMS developed at the department of Geomatics, University of Calgary in early 1990's. Recently and newer version of the VISAT^{TM} has been developed by Absolute Mapping Solution Inc. In this paper we report the task of calibrating boresight parameters of the attached cameras. The main focus will be on the inter-sensor calibration. Pre-calibration preparations are discussed. Camera and system calibration procedures are illustrated with emphasis on practical implementation aspects. Different processing scenarios are tested and commented. Finally, conclusions are drawn.

2. PRECALIBRATION PROCESS

System calibration procedures involve the estimation of the spatial relationship between mapping sensor (e.g. camera) and the navigation sensor (i.e. INS/DGPS). This relationship can be subdivided into linear and angular offsets. The linear offset can be measured using traditional surveying methods by total station or steel tapes. While the estimation of misalignment angles between the camera and the INS is done by comparing the INS rotation matrix R_b^m (between the INS body frame "b"

and the mapping frame "m") with independent R_c^m (between the camera frame "c" and the mapping frame "m") as an aerial triangulation output (Wegmann and et. al., 2004). More rigorously, total system calibration can be performed simultaneously using bundle adjustment procedures, which estimates both linear and angular offsets (e.g. Yastikli 2004) as well as their accuracy estimates. The later technique has been applied.

In all approaches, it is required to establish an accurate, rich, and well distributed control field, similar to Figure 1. This is usually done using terrestrial surveying techniques. High precision surveying techniques and instruments are used, which yield to accuracy in the millimetre level or even better.

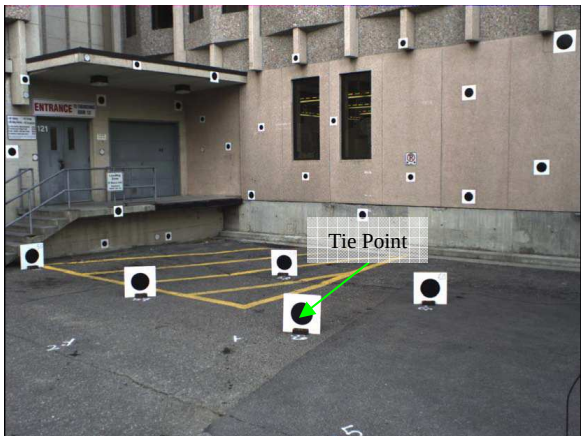

Figure 1: Control Field for VISAT MMS System Calibration

Control field must be computed in the same coordinate frame of the INS/DGPS output. Forty-six (46) control points have been established in addition to 14 tie points were temporarily fixed during the calibration session to enhance the geometry. It goes without saying that the control points must be spatially well distributed to enhance the model geometry and consequently its photogrammetric solution accuracy.

The established baseline, for photogrammetric target surveying, must be occupied by GPS receivers if possible depending on GPS signal availability. It is not always possible to occupy baseline points when control points are established near a relatively tall building to get good intersection geometry. In such case, another base line in open sky must be fixed. Later on, a terrestrial network should be run to connect baselines which can follow the traditional control network hierarchy (i.e. triletration, triangulation, hybrid, or traverse). Hybrid networks are preferred for higher degree of freedom and better accuracy. Network adjustment results shows that the standard deviation of the control points is around 1mm. Control network adjustment can be done in one of the following frames:

- Earth Fixed Coordinate Frame (EFCF)
- Universal Transverse Mercator (UTM)

Independent camera calibration has been performed by the digital photogrammetry research group (DPRP) at the University of Calgary, based on bundle adjustment with self calibration using both point and linear features. Laboratory camera calibration has been undertaken in a controlled environment. For complete description of the method used, the reader can refer to Habib et. al., 2002; Habib and Morgan, 2003 and 2004. They also investigated camera stability issues. Two sets of calibration parameters are available (Two days) with the conclusion that the cameras are fairly stable. During our processing, only one parameter set was considered due to camera stability. It is not a good practise to take average of the two data sets. One can select one calibration set as they are equivalent and will yield to the same object space coordinates.

The used mathematical model for radial lens distortion applied in camera calibration is given in equation 1.

$$\Delta x_{RLD} = x[K_1(r^2 - r_o^2) + K_2(r^4 - r_o^4) + K_3(r^6 - r_o^6)]$$
$$\Delta y_{RLD} = y[K_1(r^2 - r_o^2) + K_2(r^4 - r_o^4) + K_3(r^6 - r_o^6)] \quad (1.)$$

$$\Delta x_{RLD} = x[K_1(r^2 - r_o^2) + K_2(r^4 - r_o^4) + K_3(r^6 - r_o^6)]$$
$$\Delta y_{RLD} = y[K_1(r^2 - r_o^2) + K_2(r^4 - r_o^4) + K_3(r^6 - r_o^6)] \quad \mathbf{1}$$

Where $r = \sqrt{(x - x_p)^2 + (y - y_p)^2}$, and r_o is an arbitrary value taken as 1mm. K1, K2 and K3 are the radial lens distortion parameters, xp and yp are the image coordinates of the principal point, x and y are the image coordinates of the measured point. The term K1 alone will usually suffice in medium accuracy applications. The inclusion of the K2 and K3 terms might be required for higher accuracy and wide-angle lenses. Hence VISAT cameras has a single lens, de-centric lens distortion was not applicable. Camera CCDs are square and thus affine distortions are neglected. This model is claimed to have much computational stability and less noise dependency. This model is different from the model used in system calibration software in which r_o= 0. This makes the K1 output is not directly comparable.

The motivation behind performing individual camera calibration and not estimating camera internal orientation parameters (IOPs) during boresight calibration was due to the existence of significant correlation between the boresight and the camera IOP (Heipke, et. Al., 2001). This makes the estimation of both parameters sets in one session is suspected. Both scenarios were tested. In general, it is advisable to perform camera calibration prior to system calibration, assuming that the cameras are stable and the mounting process will not alter the camera IOPs. Moreover, camera IOPs might change under actual test conditions (Meier, 1978).

3. MATHEMATICAL MODEL

Equation $\mathbf{r}_i^{cf} = \mathbf{r}_o^{cf}(t) + R_c^{cf}(t)\left[\lambda_i \mathbf{r}^c - \mathbf{a}_b^c\right]$ 2 is the basic mathematical model for the mapping process of MMS either being aerial or land-based. It is simple and based on simple vector summation.

$$\mathbf{r}_i^{cf} = \mathbf{r}_o^{cf}(t) + R_c^{cf}(t)\left[\lambda_i \mathbf{r}^c - \mathbf{a}_b^c\right] \quad \mathbf{2}$$

Where

$\mathbf{r}_i^{cf}$ is the 3-D coordinate vector of point (i) in the computational frame (cf-frame)

$\mathbf{r}_o^{cf}(t)$ is the interpolated coordinate vector of the navigation sensors (INS/DGPS) in the cf-frame

λ^i is the scale factor corresponding to point (i)

$\mathbf{R}_c^{cf}(t)$ is the interpolated rotation matrix between the camera frame (c-frame) and the cf-frame

(t) is the time of image capture

$\mathbf{r}^c$ is the corrected image coordinate measurement vector

$\mathbf{a}_b^c$ is the vector from the camera to the body frame, measured in the c-frame

Re-writing the previous vector form in a matrix form, one gets the following system of equations.

$$\begin{bmatrix} X \\ Y \\ Z \end{bmatrix}_i = \begin{bmatrix} X_o \\ Y_o \\ Z_o \end{bmatrix} - R_c^{cf} \begin{bmatrix} a \\ b \\ c \end{bmatrix} + \lambda_i R_c^{cf} \begin{bmatrix} x \\ y \\ -f \end{bmatrix} \qquad \mathbf{3}$$

The rotation matrix R_c^{cf} can be further analyzed depending on the computational frame (either local level frame [l] or earth fixed coordinate frame [e]) into:

$$R_c^{cf} = R_b^l R_c^b \parallel R_l^e R_b^l R_c^b \qquad \mathbf{4}$$

The rotation matrix R_l^b can be computed based on roll, pitch azimuth parameterization (usually used in navigation) as follows:

$$R_l^b = R_2(r) R_1(p) R_3(-a) \qquad \mathbf{5}$$

Where r, p, and a are system roll, pitch, and azimuth respectively. [1, 2, and 3] are rotation about x, y, and z respectively. Additionally the boresight rotation matrix R_b^c can be computed as $R_b^c = R^* R_2(\Delta r) R_1(\Delta p) R_3(-\Delta a)$ 6.

$$R_b^c = R^* R_2(\Delta r) R_1(\Delta p) R_3(-\Delta a) \qquad \mathbf{6}$$

Where:

$$R^* = \begin{bmatrix} 1 & 0 & 0 \\ 0 & 0 & 1 \\ 0 & -1 & 0 \end{bmatrix}$$

$\Delta r, \Delta p, \Delta a$ are boresight angles, see Figure 1. R^* matrix is based on coordinate system definition of both body frame (x-right, y-forward, z-up) and camera frame (x aligned with image rows-right, y aligned with image column-up, z completes right handed coordinate system).

Finally:

$$R_c^{cf} = \begin{pmatrix} r_{11}^* & r_{12}^* & r_{13}^* \\ r_{21}^* & r_{22}^* & r_{23}^* \\ r_{31}^* & r_{32}^* & r_{33}^* \end{pmatrix} \qquad \mathbf{7}$$

The corresponding collinearity conditions, which includes the system calibration parameters enabling their estimation within bundle adjustment framework:

$$x = -f \frac{r_{11}^*(X - X_o) + r_{12}^*(Y - Y_o) + r_{13}^*(Z - Z_o) + a}{r_{31}^*(X - X_o) + r_{32}^*(Y - Y_o) + r_{33}^*(Z - Z_o) + c}$$

$$y = -f \frac{r_{21}^*(X - X_o) + r_{22}^*(Y - Y_o) + r_{23}^*(Z - Z_o) + b}{r_{31}^*(X - X_o) + r_{32}^*(Y - Y_o) + r_{33}^*(Z - Z_o) + c} \qquad \mathbf{8}$$

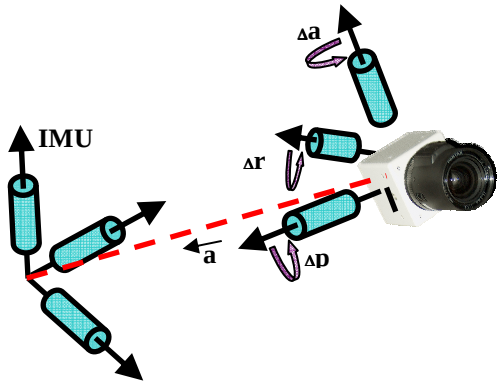

Figure 2: Relation between Navigation and Mapping Sensors

As mentioned earlier, the accuracy of mobile mapping depends on the accuracy of navigation solution, camera/system calibration, image measurement noise, and time synchronization between data streams. To understand the error budget, 10 points were simulated 5-50 m away from cameras. Errors are simulated each for accuracy governing element. Figure 3 summarizes the introduced error to each element and its corresponding percentage effect on the RMS on the 3D mapping accuracy. It is clear that some errors have insignificant effect (e.g. system roll, camera roll, and lens distortion) and some others have major contribution (e.g. system position, base length in x direction, and shift of the principle point in x direction) on the mapping accuracy. Both system synchronization and image measurement noise were not included. The total RMS 3D mapping accuracy with all introduced errors is 35cm.

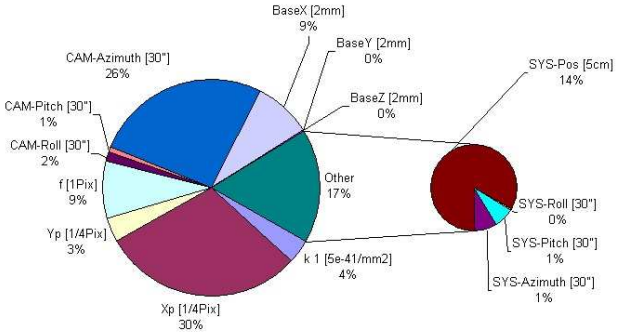

Figure 3: Error Contribution to Mapping Accuracy

4. CALIBRATION SESSION

Before performing the experiment, the calibration session has been carefully designed based on the extension of the control field, cameras distribution, and camera field of view. The goal of such design is to have the control points well distributed within the image space. Nine (9) system positions have been designed and assigned coordinates with respect to façade local coordinate system as shown in figure Figure 4. At the time of the calibration, the van was brought to the pre-designed locations marked on the ground.

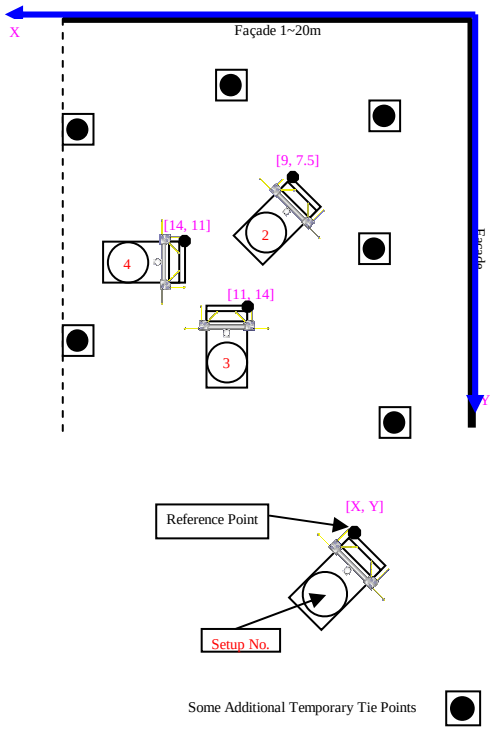

Figure 4: Example of the Executed Van Positions

To obtain the best system calibration accuracy, enhanced navigation solution must be available. If the GPS signal are blocked (e.g. obstructed by surrounding building), the INS will be working as a stand alone and the accuracy of navigation solution will be degraded since no external aiding is available. To overcome this problem, a prism was fixed at known lever arm to the INS centre. At each van location, the prism coordinates were surveyed from fixed base station using total station. The start and end time of each van location were recorded.

The surveyed positions acts as a coordinate update which were processed together with the INS signal, using the University of Calgary's AINS™ software, an Aided Inertial Navigation System Toolbox for MatLab® (Shin and El-Sheimy 2004) after applying Non-Holonomic Constraints (NHCs), backward filtering/smoothing and Odometer Derived-Velocities (ODV) as update measurements. System position and attitude are interpolated at the image exposure times in each van location.

5. COMPUTATION FRAMES

Similar to the control network adjustment, the calibration can be done in one of the following frames:

- Earth Fixed Coordinate Frame (EFCF)

In this case all the coordinates are transformed to EFCF and the attitudes are multiplied by the rotation matrix between the local level frame and the EFCF. The local level frame is defined as X = Easting, Y=Northing, and Z = Up.

$$R_l^e = R_3(-90-\lambda).R_1(\varphi-90)$$

$$R_l^e = \begin{bmatrix} -\sin\lambda & -\sin\varphi\cos\lambda & \cos\varphi\cos\lambda \\ \cos\lambda & -\sin\varphi\sin\lambda & \cos\varphi\sin\lambda \\ 0 & \cos\varphi & \sin\varphi \end{bmatrix} \qquad 9$$

Where ϕ and λ represent the geographic coordinates of the system as defined by the INS center.

The INS attitudes are used without any correction. EFCF was adopted as adjustment fame for our computations. Once the adjustment has converged, the results can be then transformed back to the mapping frame for better understanding of the results.

- Universal Transverse Mercator (UTM)

The adjustment can be also done in the UTM projected coordinates. The INS azimuth is with respect to the local (north) meridian where the system was aligned (initial alignment) while control network is aligned with zone central meridian. Therefore, INS azimuths must be corrected due to convergence of meridians. The computation of the convergence of meridians can be can be found in Borre (web site) and Nassar 1994.

This correction is sever (up to 3°) at the zone border and high latitudes. In Calgary, the latitude is 51° and the Longitude is around (-114°). The zone central meridian is -117° (UTM zone number 11). Therefore the meridian convergence is 2.23°.

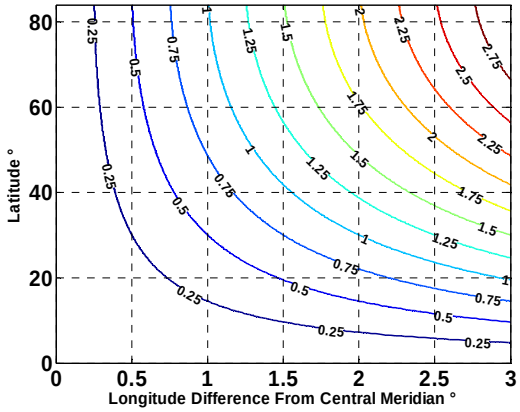

Figure 5 shows convergence of meridian contour lines for quarter of UTM zone (symmetric in both directions). It must be stressed out here that the bundle adjustment is not sensitive to azimuth systematic error. Only random error will be visible in the standard deviation of the estimated parameters. Systematic error will be totally absorbed by the estimated parameters yielding a wrong calibration set.

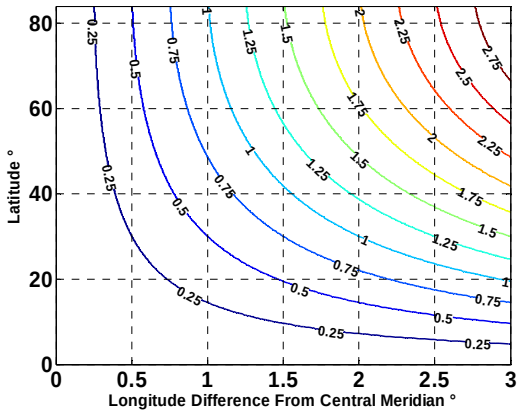

Figure 5: Convergence of Meridian contour Lines

Useful remarks on correction necessary when using UTM as an adjustment frame of airborne MMS can be found in (Jacobsen, 2003). Regardless the adopted adjustment frame, the following data elements are involved in the adjustment:

- Cameras calibration parameters.

- Approximate value for boresight angles from design.
- Interpolated system positions.
- Interpolated system attitudes.
- Image measurements
- Control points coordinates

During the 3D computation in the UTM coordinate frame, the INS azimuth must be corrected for the meridian convergence ($\Delta\alpha$) as follows:

Corrected azimuth = INS azimuth - $\Delta\alpha$ **10**

Figure 6 shows cameras distribution in one of the enclosures of VISAT^{TM}. The cameras are Kodak KAI-2020 camera. The camera has a 1600×1200pixel CCD array, and a pixel size of 7.4 microns. The camera focal length is 1700 microns. The base distance between the two camera enclosures is 2.25 metres.

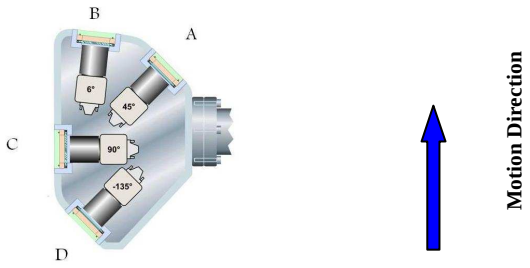

Figure 6: VISAT Imaging System (Left Enclosure)

6. EXPERIMENTS

The main objective of this paper is to obtain system calibration parameters which yield to the optimum mapping accuracy. Five processing scenarios have been tested. To check the accuracy of each calibration set, an independent check based on established ground control points were used. Twenty (20) Ground control points have been established using DGPS. Manholes, rain gutters, road signs, and lane line marking were chosen as control points and were each occupied by GPS receiver for 3 minutes static survey. These points must be checked if they appear in at least two images. Image measurements for control points were measured, using the VISAT^{TM} station using the two front cameras only (B in Figure 6). For each scenario, the 3D coordinates as well as the corresponding parallax were computed using forward intersection. The RMS of the differences between the 3D coordinates, computed based on a specific system calibration scenario, and their corresponding reference value from DGPS survey were computed for easting, northing, elevation, 2D, and 3D.

The first scenario estimates both boresight and camera interior orientation parameters (IOP) which assumes no prior camera calibration has been performed. As mentioned before, camera calibration used different radial distortion model from those used in equation

$$\Delta x_{RLD} = x[K_1(r^2 - r_o^2) + K_2(r^4 - r_o^4) + K_3(r^6 - r_o^6)]$$
$$\Delta y_{RLD} = y[K_1(r^2 - r_o^2) + K_2(r^4 - r_o^4) + K_3(r^6 - r_o^6)] \quad 1.$$

Therefore, K1 value can not be introduced as fixed value. To do similar effect, image measurements were corrected based on k1 value and the corresponding math model as scenario II, named as distortion free scenario. Using the corrected image measurements, two scenarios were tested in which the focal length and the principle point (PP) shift were estimated respectively (scenarios IV, and V respectively). Last scenario (III), estimates the K1 value in addition to system calibration parameters.

In all cases, image measurements have to be corrected from different kinds of distortions before using them in the 3D computation. The mapping accuracy of scenarios (II, IV, V) was recomputed based on the distortion model in equation

$$\Delta x_{RLD} = x[K_1(r^2 - r_o^2) + K_2(r^4 - r_o^4) + K_3(r^6 - r_o^6)]$$
$$\Delta y_{RLD} = y[K_1(r^2 - r_o^2) + K_2(r^4 - r_o^4) + K_3(r^6 - r_o^6)] \quad 1$$

with ro = 0.0 (i.e. the same as in system calibration). This was done to check if the two distortion models (ro = 0.0 or ro=1.0 mm) will yield to the same accuracy.

7. RESULTS

Table 1 lists the statistics for the different tested scenarios for parallax, easting, northing, elevation, 2D, and 3D. Mean, maximum, minimum, and RMS are computed. Among the different tested scenarios, scenario I, where all the IOPs were estimated in addition to the estimated boresight parameters, yielded the most accurate results. The improvement is not significant. However, this was surprising but may be due to the number and the geometry of both van and control points which strengthened the photogrammetric network and reduced the correlation between the different groups of estimated parameters. This scenario has the advantage over performing a prior camera calibration as this avoids camera instability due to mounting process and the estimation is under field conditions.

		Mean	Max.	Min.	RMS
ALL IOP Estimated (I)	P	0.000	0.002	0.001	0.001
	E	-0.134	0.122	-0.016	0.062
	N	-0.126	0.039	-0.014	0.042
	H	-0.055	0.077	0.033	0.049
	2D	0.003	0.156	0.059	0.075
	3D	0.030	0.171	0.081	0.090
Distortion Free (II)	P	0.000	0.003	0.001	0.002
	E	-0.142	0.120	-0.022	0.068
	N	-0.134	0.033	-0.013	0.044
	H	-0.062	0.076	0.029	0.047
	2D	0.005	0.146	0.066	0.081
	3D	0.022	0.149	0.084	0.094
K1 Estimated (III)	P	0.000	0.003	0.001	0.001
	E	-0.140	0.118	-0.021	0.068
	N	-0.134	0.031	-0.013	0.044
	H	-0.061	0.076	0.030	0.048
	2D	0.004	0.143	0.066	0.081
	3D	0.023	0.147	0.084	0.094
Focal length Estimated (IV)	P	0.000	0.003	0.001	0.001
	E	-0.137	0.087	-0.021	0.064
	N	-0.135	0.030	-0.012	0.043
	H	-0.059	0.077	0.031	0.048
	2D	0.007	0.140	0.062	0.077
	3D	0.027	0.147	0.082	0.091
PP. Shift Estimated (V)	P	0.000	0.003	0.001	0.002
	E	-0.140	0.109	-0.020	0.065
	N	-0.128	0.030	-0.013	0.043
	H	-0.061	0.076	0.030	0.048
	2D	0.004	0.142	0.063	0.078
	3D	0.024	0.145	0.083	0.092

Table 1: Mapping Accuracy Statistics for Different Processing Scenarios.

Comparing the results of different tests, it can be also concluded that our estimation of all parameters are very stable although the estimation of parameters from different scenarios yielded different values for the same parameter. The maximum difference between different scenarios is listed in Table 2.

	Item	Max. Difference
Camera Boresight	X	2mm
	Y	2cm
	Z	3mm
	Roll	10”
	Pitch	10’
	Azimuth	3’
Camera IOPs	Focal length	3pixels
	PP shift x	0.25pixel
	PP shift y	0.5pixel

Table 2: Difference in Estimation with Different Processing Scenarios

Change in one parameter may be absorbed by another parameter yielding to the same object space. It was necessary to test if the results from the two radial distortion models (ro = 0.0 or ro=1.0 mm) are equivalent. After estimating the boresight parameters from scenarios II, IV, and V, the mapping accuracy was rechecked with the other distortion model. It was observed that the two models yielded to almost identical results. Table 3 shows such results.

		Mean	Max.	Min.	RMS
Distortion Free (II)	P	0.000	0.003	0.001	0.002
	E	-0.142	0.116	-0.023	0.068
	N	-0.139	0.034	-0.012	0.045
	H	-0.061	0.075	0.029	0.047
	2D	0.006	0.146	0.066	0.081
	3D	0.022	0.149	0.084	0.094
Focal length Estimated (IV)	P	0.000	0.003	0.001	0.001
	E	-0.137	0.087	-0.021	0.064
	N	-0.140	0.031	-0.012	0.044
	H	-0.059	0.077	0.031	0.048
	2D	0.009	0.143	0.063	0.077
	3D	0.026	0.148	0.082	0.091
PP. Shift Estimated (V)	P	0.000	0.003	0.001	0.002
	E	-0.140	0.105	-0.021	0.065
	N	-0.133	0.030	-0.013	0.043
	H	-0.061	0.076	0.030	0.048
	2D	0.003	0.142	0.063	0.078
	3D	0.024	0.146	0.082	0.092

Table 3: Mapping Accuracy Statistics for Different Processing Scenarios (ro = 0.0)

In general, we observed that the computed standard deviations for the estimated parameters from bundle adjustment were pessimistic when compared to the error analysis presented in section 3 and the obtained results for absolute 3D mapping accuracy. It must be stressed out here that our results and conclusions are based on mapping from the two front cameras. There is no guarantee that the boresight quality is the same for all cameras as network connectivity was different for each camera. It is required to have a special control field to have similar connectivity for all cameras.

8. SUMMARY AND CONCLUSIONS

Mobile mapping systems are effective tools for collecting up-to-data GIS features. They provide fast and cost effective mapping solution. The delivered accuracy is function of navigation solution accuracy, system calibration, and mapping sensor calibration. This paper deals with system calibration in which the relation between camera and navigation sensor are estimated. Different processing scenarios were tested. The accuracy based on an independent check points were computed. The difference between the different scenarios is insignificant, provided that the calibration was done based on sufficient and well distributed number of van setups in addition to accurate, spatially distributed control filed. Finally, bundle adjustment accuracy measures for the estimated parameters were not realistic and the evaluation of the quality must be based on check point analysis.

9. ACKNOWLEDGEMENTS

The authors wish to thank the Canadian GEOIDE NCE and NSERC for their financial support. Cameron Ellum is acknowledged as the co-author of the Addingham Simulation/Adjustment software suite used for data processing. Dr. Ayman Habib and his team are also acknowledged for performing camera calibration.

10. REFERENCES

Borre K., Ellipsoidal geometry and conformal mapping, Aalborg University, Department of communication technology.

[website]http://kom.aau.dk/~borre/masters/frames/notes.pdf (last accessed 2007-11-09)

Ellum, C.M. and El-Sheimy, N. (2005). Integrating photogrammetry and GPS at the measurement-level. Proceedings of ION GNSS 2005. September 13-16, Long Beach, CA, USA.

El-Sheimy, N (1996). The Development of VISAT - A Mobile Survey System for GIS Applications, Ph.D. thesis, The University of Calgary, UCGE Report No. 20101 (http://www.geomatics.ucalgary.ca/Papers/Thesis/KPS/96.20101.NEl-Sheimy.pdf).

El-Sheimy, N., (1996). A Mobile Multi-Sensor System For GIS Applications In Urban Centers. The International Society for Photogrammetry and Remote Sensing (ISPRS) 1996, Commission II, Working Group 1, Vol. XXXI, Part B2, pp. 95-100, Vienna, Austria, July 9-19.

El-Sheimy, N., (2005). An Overview of Mobile Mapping Systems. FIG Working Week 2005 and GSDI-8, Cairo, Egypt April 16-21.

Grejner-Brzezinska, D. A., (1999). Direct Exterior Orientation of Airborne Imagery with GPS/INS system: Performance analysis, Navigation, Vol. 46, No. 4, pp. 261-270.

Grejner-Brzezinska D., Li, R., Haala N., Toth C., (2002). Multi-Sensor Systems for Land-Based and Airborne Mapping: Technology of the Future?. ISPRS Commission II, WGII/1, China August 20-23, 2002.

Habib, A., Lee, Y., Morgan, M., 2002. “Bundle Adjustment with Self-Calibration using Straight Lines.” Photogrammetric Record Journal, 17(100):635-650, October 2002.

Habib, A., and M. Morgan, 2003, Automatic Calibration of Low-Cost Digital Cameras, Journal of Optical Engineering, 42(4):948-955, April 2003.

Habib, A., and M. Morgan, 2004, Stability analysis and geometric calibration of off-the-shelf digital cameras, Photogrammetric Engineering and Remote Sensing, 71, 6, June, 2005, p 733-741

Heipke, C., Jacobsen, K., Wegmann, H.(2001): The OEEPE-Test on Integrated Sensor Orientation – Analysis of Results, OEEPE-Workshop Integrated Sensor Orientation, Hannover Sept. 2001

Jacobsen, K., 2003, System Calibration for Direct and Integrated Sensor Orientation, Theory, Technology and Realities of Inertial/GPS Sensor Orientation. ISPRS WG I/5, Barcelona, 2003, 6S., CD .

Meier, H.-K. (1978), The Effect of Environmental Conditions on Distortion, Calibrated Focal Length and Focus of Aerial Survey Cameras, ISP Symposium, Tokyo 1978.

Nassar, M. M., Advanced geometric geodesy, 1994, Lecture notes, Faculty of Engineering, Ain Shams University, Cairo, Egypt.

Schwarz K. P., El-Sheimy N., (2004). Mobile Mapping Systems – State of The Art and Future Trends, ISPRS Commission 5, Istanbul, Turkey.

Shin, E-H. and El-Sheimy N., (2004). Aided Inertial Navigation System (AINS™) Toolbox for MatLab® Software. Mobile Multi-Sensor Systems research group, the University of Calgary, Canada.

http://www.mms.geomatics.ucalgary.ca/Research/ research.htm

(Accessed 2 April 2006).

Skaloud J. (1999). Problems in Direct-Georeferencing by INS/DGPS in the Airborne Environment. ISPRS Workshop on "Direct versus Indirect Methods of Sensor Orientation", WG III/I, Barcelona, 1999.

Wegmann H., Heipke C., and Jacobsen K, (2004). Direct Sensor Orientation Based on GPS Network Solutions. ISPRS Commission I, WG V, Istanbul, Turkey.

Yastikli N. (2004). The Effect of System Calibration on Direct Sensor Orientation. ISPRS Commission I, WG V, Istanbul, Turkey.